Exploring Biomimetic Stiffness Modulation and Wearable Finger Haptics for Improving Myoelectric Control of Virtual Hand

Hong Zeng, *Member, IEEE*, Weijie Yu, Dapeng Chen, *Member, IEEE*, Xuhui Hu, *Graduate Student Member, IEEE*, Dingguo Zhang, *Senior Member, IEEE*, and Aiguo Song, *Senior Member, IEEE*

***Abstract*— The embodiment of virtual hand (VH) by the user is generally deemed to be important for virtual reality (VR) based hand rehabilitation applications, which may help to engage the user and promote motor skill relearning. In particular, it requires that the VH should produce task-dependent interaction behaviors from rigid to soft. While such a capability is inherent to humans via hand stiffness regulation and haptic interactions, yet it have not been successfully imitated by VH in existing studies. In this paper, we present a work which integrates biomimetic stiffness regulation and wearable finger force feedback in VR scenarios involving myoelectric control of VH. On one hand, the biomimetic stiffness modulation intuitively enables VH to imitate the stiffness profile of the user's hand in real time. On the other hand, the wearable finger force-feedback device elicits a natural and realistic sensation of external force on the fingertip, which provides the user a proper understanding of the environment for enhancing his/her stiffness regulation. The benefits of the proposed integrated system were evaluated with eight healthy subjects that performed two tasks with opposite stiffness requirements. The achieved performance is compared with reduced versions of the integrated system, where either biomimetic impedance control or wearable force feedback is excluded. The results suggest that the proposed integrated system enables the stiffness of VH to be adaptively regulated by the user through the perception of interaction torques and vision, resulting in task-dependent behaviors from rigid to soft for VH.**

Manuscript received November 30, 2021; revised March 29, 2022 and April 27, 2022; accepted June 5, 2022. Date of publication June 8, 2022; date of current version June 21, 2022. This work was supported by the National Natural Science Foundation of China under Grant 62173089, Grant 62003169, Grant 92148205, and Grant 61773219. *(Corresponding author: Hong Zeng.)*

This work involved human subjects or animals in its research. Approval of all ethical and experimental procedures and protocols was granted by the ethic committee of Southeast University under Application No. 2019ZDSYLL001-P01, and performed in line with the Declaration of Helsinki.

Hong Zeng, Weijie Yu, Xuhui Hu, and Aiguo Song are with the State Key Laboratory of Bioelectronics and the Jiangsu Province Key Laboratory of Remote Measurement and Control, School of Instrument Science and Engineering, Southeast University, Nanjing 210096, China (e-mail: hzeng@seu.edu.cn).

Dapeng Chen is with the School of Automation, Nanjing University of Information Science and Technology, Nanjing 210044, China.

Dingguo Zhang is with the Department of Electronic and Electrical Engineering, University of Bath, Bath BA2 7AY, U.K.

Digital Object Identifier 10.1109/TNSRE.2022.3181284

***Index Terms*— Electromyography, virtual reality, impedance control, biomimetic stiffness modulation, wearable finger haptics, task-dependent interaction behavior.**

I. Introduction

OVER the decades, the virtual reality (VR) techniques have shown their advantages for motor impaired people in rehabilitation applications, by offering goal-oriented tasks and enriched sensorimotor experiences, which are otherwise unfeasible in common therapies [1]–[5]. In particular, with regard to VR-based hand rehabilitation applications involving a virtual hand (VH), researchers have recently reached a consensus that VH should not only mimick the appearance and functionality of human hands, but also demonstrate versatile interaction behaviors [6]–[8]. Demonstrating versatile behaviors, especially those mimic the characteristics unique to human hand interaction behaviors, would enable VH to be embodied by the user (i.e., operated and perceived as his/her own hand during interactions), which may facilitate the activation of brain networks involved in sensorimotor learning and thus promote the hand function recovery.

Here, to implement a natural, intuitive and hands-free active control of VH, we adopt the myoelectric interface, since it conforms to the original neuromuscular pathway and directly addresses muscle activation patterns for rehabilitative training [9]–[12]. Moreover, we focus on VH's physical interactions with the virtual environment, such as equilibrium point manipulation of a virtual object, involving both force and position control. Developing such systems, instead of ones with free-space position-based control [9], [13], could undoubtedly enhance the immersive experience and the realism in VR [14], [15]. A well-known strategy that can regulate the physical interaction is the impedance model based control method. With the prior knowledge about well-studied VR tasks, the stiffness of impedance model could be set deliberately to induce the desired rigid or delicate soft elastic interactive behaviors. For instance, grasping necessitates compliant operation, while accurate position tracking under disturbances requires stiff operation. Nevertheless, the manual planning and adjusting of the stiffness gains for a new or complex VR task are difficult and time-tedious. As a consequence, existing studies [14],

[16], [17] fail to adaptively produce task-desired interaction behaviors for VH, which would probably ruin its embodiment.

As a matter of fact, the adaptive hand stiffness regulation is inherent to the human neuromuscular system in daily activities involving physical interactions with human hands [18]. In specific, the stiffness around a degree of freedom is directly modulated by co-contracting the corresponding agonist-antagonistic muscle pairs to realize rigid/soft interaction, which takes place naturally from task to task and during a single task execution. Within this context, the impedance control paradigm with biomimetic stiffness modulation has the potential for enabling VH to mimick the human hands' capability of adaptive stiffness modulation in various interaction scenarios.

Moreover, in response to externally imposed hand displacements, the human central nervous system integrates multi-sensory feedback to regulate hand impedance for ensuring task requirements [19]. Such a fact suggests that biomimetic impedance control may provide only a partial and open-loop solution to the problem of lacking adaptive task-dependent behaviors in existing VH studies; high-quality sensory feedback congruent to VH actions is further required for obtaining a good perception of the VH interaction with environment, so as to enable effective stiffness modulation in a closed-loop way. Moreover, the kinesthetic feedback has been found to be a dominant modality in promoting motor learning [20]. Thereby, regarding to rehabilitation applications for which our VH system is targeted in the future, the wearable finger haptic device providing the kinesthetic feedback would remain the first choice, which offers an intuitive way to give the user realistic sense of touch.

In this paper, to overcome the deficiency of failing to offer adaptive task-dependent behaviors for VH in current studies, we aim at establishing a solution that subsumes the advantages of wearable haptic devices and biomimetic stiffness modulation. Specifically, an integrated bidirectional interface is proposed for improving the myoelectric-controlled VH, which combines the biomimetic impedance control paradigm and wearable finger force feedback in a closed-loop way. Firstly, the joint stiffness profiles of the user hand are estimated from muscular activations in real time, and then used to adjust the stiffness gain in the impedance control model for generating task-desired VH finger movements. Moreover, a lightweight finger-worn haptic device is used to feed the VH grasp or environmental perturbation torques back to the user in an intuitive manner, which may enable the user to appropriately modulate his/her joint stiffness. The proposed integrated interface is verified with two tasks typically trained in neuromotor rehabilitation programs, which encourage the use of opposite stiffness levels, representing soft-to-rigid interaction requirements. In specific, able-bodied users controlled a one-degree-of-freedom (1-DoF) variable-impedance VH to complete two 1-DoF tasks: (1) a grasping task which requires to minimize contact torques between VH and the object in VR environment while ensuring successful and robust grasps. (2) a trajectory tracking task which requires to track a specified trajectory with VH while experiencing random perturbations. The achieved performance is presented in comparison with reduced versions of the integrated system, where either biomimetic impedance control or wearable feedback is excluded.

II. Related Work

Toward imitating the stiffness regulation feature of humans for slave robot control, the biomimetic stiffness modulation has been proposed recently in teleoperation [21]–[24]. In such a control paradigm, the master-side human joint stiffness is estimated in real-time from muscular activations with electromyography (EMG) signals, and then mapped to the slave robot, introducing advantages such as safety, energy efficiency and stability for teleoperation [21]–[24].

Most biomimetic impedance control studies have employed the visual feedback [24], [25], while only a few recent efforts have explored the benefits of haptic feedback in biomimetic impedance control for robotic teleoperation. Studies in [22], [26] have utilized the grounded mater robot to render the force feedback coming from the remote robot, when completing the classic peg-in-hole task with a biomimetic impedance control paradigm. It has been demonstrated that the perception of task environment could be enhanced with this kind of grounded haptic devices, though at the expense of workspace size. To overcome such an limitation, studies in [23], [27], [28] have paired the biomimetic impedance control with the wearable haptics, which provide feedback on the force of robotic hand or dual-arm closure with mechanotactile stimulations (e.g., skin stretch and squeeze) applied to the upper arm of the user. The addition of such a wearable haptic feedback has been shown to enable effective modulations of force in grasping or peg-in-hole task, when visual cues are limited or unavailable. Nevertheless, since the physical contact force between the slave hand/end-effector and the environment is not rendered directly but converted into tactile cues, and displayed on the user arm rather than the user hand at the master side [23], [27], [28], such an arm-worn haptic interface may not be intuitive enough, and even might serve as distractions or cues difficult to interpret [28].

Regarding the VR-based hand rehabilitation applications, hand-worn haptic devices represent a great opportunity since they provide intuitive cutanoeus feedback on fingerpad, and vast studies have shown that congruent haptic sensory afferents can guide neuroplasticity toward restoration of motor functions [3], [5], [20]. Although commercially-available glove-type haptic displays (e.g.,CyberGrasp, HaptX) provide realistic feeling of touch in VR, they are nonetheless quite heavy, cumbersome and too expensive in community/home rehabilitation terms. Recently, there is an increasing trend of developing wearable finger haptic devices that are compact, comfortable and inexpensive [29], [30], each focusing on specific features of haptic rendering (e.g., force feedback [31], curvature [32], surface orientation [33], surface texture [34]). A variety of studies [5], [29], [30] have shown that such devices could enhance the VR interaction performance, in terms of manipulation compliance, task success rate, perceived immersiveness and etc. Nevertheless, none of them has investigated whether wearable finger haptics could promote the task-dependent hand stiffness regularization for the user.

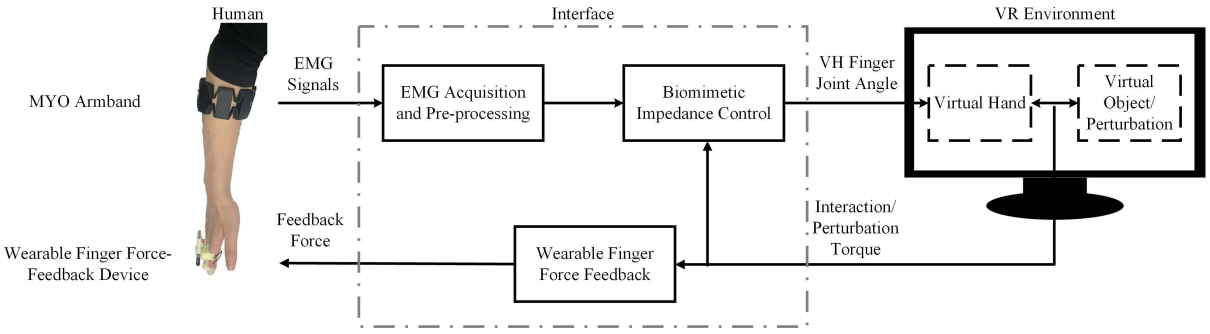

Fig. 1. The system architecture of the myoelectric-controlled VH. With the integrated interface (the dash-dotted frame), EMG signals from the subject's forearm command the VH's finger joint angle, while the subject receives force feedback of the interaction torque between VH and object or the perturbation torque.

III. Materials and Methods

A. Integrated Interface Architecture

The proposed human-VR interface (see Fig. 1) consists of three main components: the EMG acquisition and pre-processing, the biomimetic impedance control, and the wearable finger force feedback. We employ a MYO Armband to capture the major finger antagonist pair of muscular activations from the forearm. The pre-processed EMG signals are then fed into the biomimetic control module for determining the VH finger angle, which manages the rigid or soft elastic behavior of VH interacting with the virtual environment. During the interaction, the user's voluntary co-contraction of antagonist muscle pair is regulated with the perception of the VH state and the applied environment torques via vision and the finger force-feedback device.

B. EMG Signals Acquisition and Pre-Processing

The surface EMG was measured with the MYO armband worn around the forearm just below the elbow, using a 200-Hz sampling rate. The EMG signal was then full-wave rectified, smoothed with a second order low-pass Butterworth filter (cut-off frequency 5 Hz) to obtain its envelope. Before starting the experiments, the subject was instructed to exert a large and brief co-contraction, and the corresponding maximal voluntary contraction (MVC) value for each EMG channel was calculated as the average around its peak, then it was used to normalize the EMG signals online.

For both the human hand and the virtual hand, we only allowed the flexion and extension activity of the finger's metacarpophalangeal (MCP) joint, while those for the distal interphalangeal (DIP) joint and the proximal interphalangeal (PIP) joint were prohibited. It has been found in previous studies [23], [35] that the MCP joint of the finger can be modulated by the co-contraction of the major finger antagonistic muscle pair in the forearm: flexor digitorum superficialis (FDS) and extensor digitorum communis (EDC) muscles. In our study, we obtained the muscle activation of FDS by averaging the measure from electrodes pair 6-7 on the MYO armband, and the muscle activation of EDC with the electrode 3 (see Fig. 2), as suggested in [36], [37]. Hereafter, we use A_f and A_e to denote the processed antagonistic muscle pair EMG signals, which are fed into the biomimetic impedance control model described in the next section.

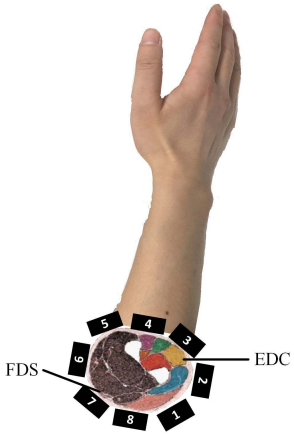

Fig. 2. MYO Armband placement with cross-section view of upper forearm muscles. The electrodes are labeled with IDs from 1 to 8, where the fourth electrode has a blue marker.

C. Biomimetic Impedance Control of Virtual Hand

In this subsection, a method for controlling a virtual hand based on the mechanical impedance of the human hand's finger movements will be illustrated. In specific, the equation of motion around the VH's MCP joint is defined as [38]:

$$\tau = M\ddot{\theta} + B\dot{\theta} + K(\theta - \theta_0) + \tau_{ext}, \tag{1}$$

where τ and τ_{ext} are the input torque to the VH finger and the external torque acting on the VH finger, respectively; θ and θ_0 are the joint angle and its equilibrium position; M, B and K are the inertia, damping and stiffness of the VH's MCP joint, respectively. Considering slow movements of the joint, the effect of inertia in the above equation could be neglected, and thus we can write

$$\dot{\theta} = -\frac{K}{B}(\theta - \theta_0) + \frac{\tau - \tau_{ext}}{B}. \tag{2}$$

To calculate the joint angle θ numerically with the above equation, the input torque τ, the stiffness K and the damping B should be modeled first with the real-time changing EMG signals. It is well known that the muscle activity is directly related to the muscular force [39]. Therefore, as in [38], the joint torque τ caused by the muscular contraction of flexors and extensors is approximated as

$$\tau = a_\tau \delta(A_f, A_e), \tag{3}$$

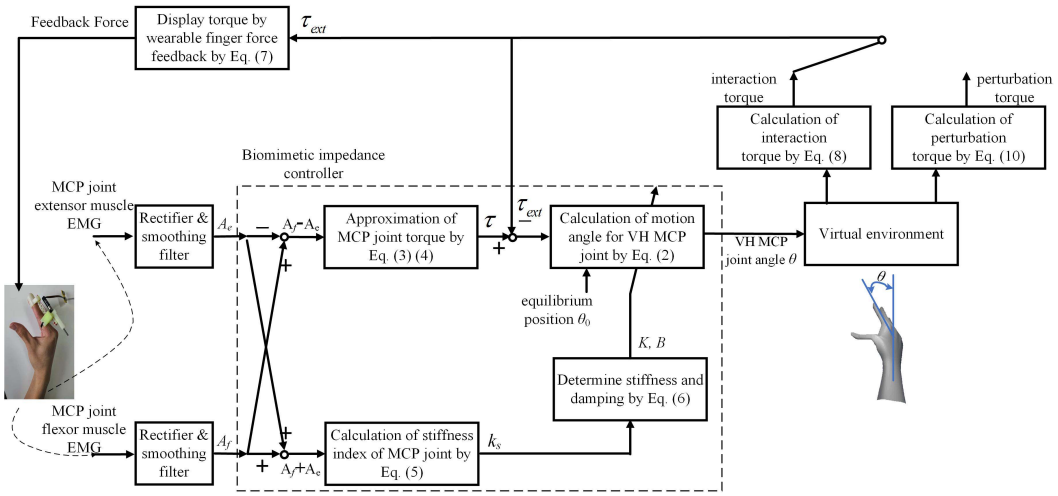

Fig. 3. The VH control diagram, where the biomimetic impedance controller is highlighted with the dashed frame.

where $\delta(A_f, A_e)$ is a function of the difference in activation of the antagonistic muscles $(A_f - A_e)$, and a_τ is the gain. On the other hand, since the force from each muscle could antagonistically affect the MCP joint torque, the stiffness index of finger's joint $k_s(A_f, A_e)$ $(k_s(A_f, A_e) \in [0, 1])$ could be modeled with a function of the summation in activation of the antagonistic muscles $(A_f + A_e)$. The exact mappings between EMG signals and $\delta(A_f, A_e)/k_s(A_f, A_e)$ are established with the following modified hyperbolic tangent functions [23]:

$$\delta(A_f, A_e) = \frac{a_\delta(1 - e^{-b_\delta(A_f - A_e)})}{1 + e^{-b_\delta(A_f - A_e)}}, \tag{4}$$

$$k_s(A_f, A_e) = \frac{a_k(1 - e^{-b_k(A_f + A_e)})}{1 + e^{-b_k(A_f + A_e)}}, \tag{5}$$

where a_δ, b_δ, a_k and b_k are constant gains to be determined during the calibration phase. Once the stiffness index $k_s(A_f, A_e)$ is obtained, the stiffness K and the damping B in equation (2) could be calculated by:

$$\begin{aligned} K &= k_s(A_f, A_e)(K_{max} - K_{min}) + K_{min}, \\ B &= 2\sqrt{K}, \end{aligned} \tag{6}$$

where K_{max} and K_{min} stand for the higher and lower bounds of VH's stiffness values, respectively; the damping B is set in this way to stabilize the system. In this manner, the stiffness and damping are made to change according to the muscle co-contraction level. Note that we does not calculate exact values of joint stiffness, the designed system relies only on detecting changes in stiffness. Fig. 3 shows the overall biomimetic impedance control system used in this study.

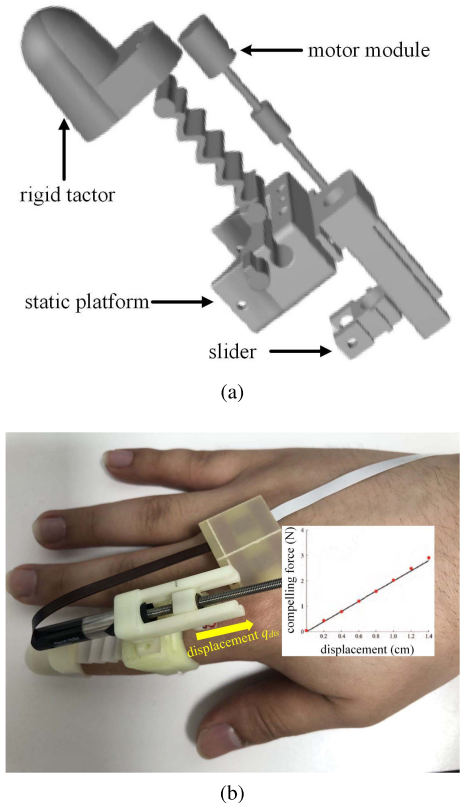

Fig. 4. The wearable finger haptic device employed in our study. (a) The device in exploded view. The compelling force is delivered by the tactor, which is driven by cables connecting it with the slider. The movement of slider is actuated with the motor module. (b) The force provided by the device is approximately linearly scaled with the displacement of slider.

D. Wearable Finger Force Feedback

In the proposed integrated interface, a custom made wearable fingertip haptic device (Fig. 4) preliminary presented by Mo *et al.* [40] provides the user with interaction/perturbation forces. It is compact, comfortable and will not impair the motion of the wearer. The device consists of a 3D-printed static platform with an adhesive connector, a motor module, a slider and a rigid tactor. The static platform which is located on the nail side of the index finger, houses a light motor module and a slider. A rigid spherical tactor that contacts with the finger pulp is connected to the static platform with a wave-shape adhesive connector, which helps to fit for subjects with various finger lengths. The tactor is also linked to the slider mounted at the spindle drive, with steel cables (0.5 mm in diameter) passing through the upper holes of the static platform and the tactor.

The motor module actuates the slider, which is constrained to slide either upward or downward by trails on the frame of the static platform. Specifically, when the motor conducts clockwise rotations, the slider will slide up to strengthen the tension of cables, rendering a compelling force by deformation of the fingerpad with the connected tactor. The wearable device weighs 34.6 g for 125 × 28 × 38 mm dimensions.

The adopted motor module consists of a DC motor (maxon 347724), an encoder (maxon 334910) and spindle drive (maxon 473645). It is controlled with a microcontroller (STMicroelectronics, STM32F103CBT6), and driven by DRV8830 from Texas Instruments Inc. The microcontroller communicates with the host PC via Bluetooth. The whole haptic device is battery powered and wireless in order to minimize interference with movements of the user.

With such a force feedback scheme, it leads to a linear mapping between the displacement of the slider and the force that the device provides (see Fig. 4(b)) [40]. The maximum linear force that could be exerted by the tactor in contact with the fingerpad was 2.91 N [40], comparable with values measured during free cutaneous exploration. Then the task interaction torques could be scaled, converted and rendered by such a haptic device. Namely, the required displacement of the slider q_{dis} is computed as follows:

$$q_{dis} = \frac{a_{scale}\tau_{ext}}{k_{map}}, \tag{7}$$

where a_{scale} is a constant found experimentally that scales and converts the task interaction torques to a desired force to be applied with haptic device, varying between 0 and 2.91 N. k_{map} is the device's inherent parameter for mapping between q_{dis} and the force provided by the device, which has been already identified experimentally in pilot study [40].

IV. Experiments

A. Experimental Setup and Subjects

Fig. 5 shows the experimental setup in our study. The subject was seated in a comfortable chair in front of the monitor while the weight of the forearm was supported on the table. Two VR interactive scenarios were developed with Unity 3D. The EMG signals were collected from the forearm via the MYO armband when the subject performed the extension and flexion of his/her index, middle, ring and little fingers together, and then translated into the VH's MCP joint angle command for interacting with a virtual object or following a reference trajectory. At the same time, subjects could see the interaction between the VH and the VR environment, as well as feel the task interaction torque with the wearable haptic device worn on the index finger under the force feedback condition.

Eight right-handed volunteers (Five males and three females, age 22-27 years) took part in the experiments. No participants claimed any limitations nor pathology that could affect force sensation or muscular activity to perform the tasks. The methods and procedures described herein were carried out in accordance with the recommendations of the ethic committee of Southeast University (2019ZDSYLL001-P01), with written informed consent obtained from all users.

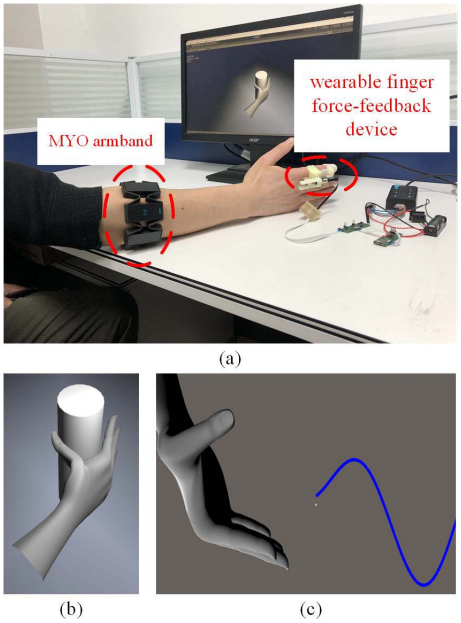

Fig. 5. Experimental setup (a) and visual representations of the grasping task (b) and the position tracking task (c) in our study.

B. Experimental Protocol

The subject first received a short introduction about the tasks and then carried out a short calibration. Afterward the subject performed the grasping task and the position tracking task in the following six conditions for VH control paradigms: 1) low stiffness (LS) with $K \equiv K_{min}$ (2.5 Nm/deg), 2) high stiffness (HS) with $K \equiv K_{max}$ (3.5 Nm/deg), and 3) biomimetic stiffness (BS) with K determined by Eq. (6), with and without the use of wearable fingertip force-feedback device (FinFF) for force feedback. Before the formal experiments, the subject was asked to get familiar with the devices and procedures. The order of these conditions was randomized within the two tasks, and the subjects were not informed on the current condition. They were also unaware that they could use co-contraction to influence the stiffness of VH. The subject performance was averaged over repetitions of the same condition.

C. Calibration

For each subject, fast calibrations for the biomimetic impedance controller was conducted in free space, where the external torque τ_{ext} in equation (2) were not taken into account. Two set of experimental trials were recorded to identify the constants (i.e., $a_\tau, a_\delta, b_\delta, a_k$ and b_k) in Eq. (3), (4) and (5). In the first set, each subject was instructed to slowly open and close the hand with visual guidance and feedback on the monitor, while the EMG signals were recorded with MYO and the MCP joint angles were simultaneously collected with a GY-25 tilt angle sensor module. There were 10 trials obtained in the first set, each trial lasted 30 seconds. For the second set, subjects were asked to perform the grasp at five different FDS and EDC co-contraction levels (10%, 30%, 50%, 70% and 90%), with visual feedback of co-contraction for steadily maintaining at the instructed

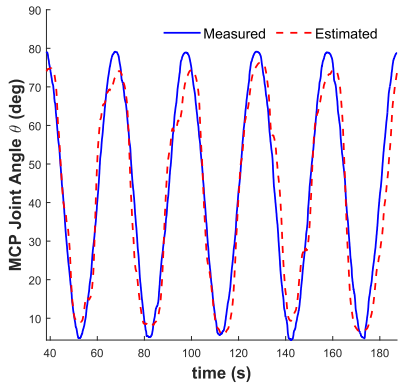

Fig. 6. Comparison between the estimated and measured angles in a typical test trial of a representative subject in the calibration phase.

stiffness levels. This set comprised 20 trials, where four trials were recorded for each level. The identification of model parameters for τ and k_s, and the corresponding finger angle and stiffness references, respectively, was performed on even numbered trials, and the odd trials were used for the evaluation. We obtained the cross-subject average normalized root-mean-squared error 16.03% and 8.76% for the angle and stiffness test trials, respectively. Fig. 6 depicts a typical angle estimation performance with the biomimetic impedance model for a representative subject in a test trial during the calibration phase. The estimated angle for VH almost corresponds with that of the subject, indicating that the biomimetic impedance model in equation (2) can express the human finger MCP joint's motions.

It is necessary to point out that we did not use angle sensor module (GY-25) during the latter two tasks, since the index finger was already worn a finger force-feedback device. We decided to avoid cumbersome configurations for the system, to allow a natural interaction.

D. Grasping Task

The first task was designed to evaluate the effectiveness of human-in-the-loop modified stiffness with interaction torque feedback for achieving compliant grasps of VH. A screenshot of this experiment can be seen in Fig. 5 (b), containing a VH and a virtual cylindroid object. In each trial, the thumb of VH always contacted with the object, and as the subject closed/opened his/her hand by moving the other four fingers, the VH generated the flexion/extension motion of user fingers to grasp the virtual object, using the biomimetic impedance control. Only the rotations of MCP joints were allowed for the other four fingers in the experiment for both user hand and VH. Once the VH contacted with the virtual object, the finger haptic device delivered force sensations to the subject. In particular, the mechanical dynamics of the cylindroid object were modeled in a simple fashion as a spring. Thereby the interaction torque between VH and object was calculated as:

$$\tau_{ext} = K_o(\theta - \theta_{obj}), \tag{8}$$

where $K_o = 3$ Nm/deg is a constant, θ and θ_{obj} denote the current MCP joint angle and the one when the contact with the object occurs, respectively. Then the external torque was fed into equation (2) together with A_f and A_e for updating θ, where the equilibrium position θ_0 was set to 0 in free space and θ_{obj} once VH contacted with the virtual object, respectively. Note that the VH and virtual object were designed to be opaque and behave as rigid bodies that have no geometric warping or distortion, therefore, the subjects could not guess the grip torque from the visual information. Successful grasp was achieved when the period during which the grip torque was greater than 7 Nm (a low bound for grasping the object) lasted more than 2.5 seconds. A fixed-distance upward-motion animation of the VH and object was displayed to the user, once he/she completed a successful grasp. The subject was asked to minimize the magnitude of the interaction torque while ensuring successful grasps. For each condition, four trials were recorded.

From a compliant and energy-efficiency interaction view, the interaction torque τ_{ext} in successful trials was chosen as the performance metric for the grasping task, since less torque applied to the virtual object means that users have promptly stopped their fingers when VH was in contact with the rigid object. Besides, it could help to minimize the fatigue in future VR-based training applications. The number of successful grasps were also recorded.

E. Position Tracking Task

The second task was aimed at assessing the efficacy of biomimetic stiffness regulation under visual-haptic feedback, for reaching a rigid position tracking behavior while experiencing random perturbations. The visual representation of the task is shown in Fig. 5 (c). A one-dimensional reference trajectory scrolled across the screen from right to left at a reasonable constant speed (Fig. 7(a)), which was determined by the following equation:

$$y_t = 12\sin\left(\frac{2\pi t}{60} + \frac{\pi}{6}\right) + 12\sin\left(\frac{4\pi t}{60} + \frac{2\pi}{3}\right) + 45 \tag{9}$$

The task parameters were chosen such that the desired trajectory covered a significant portion of workspace range and moved at a slow enough pace for the subjects to track. The motion of VH is projected to a small white dot (Fig. 5 (c)), i.e., the small white dot represents the user's VH. The user moves the VH vertically to keep it on the desired trajectory, while random perturbation torques (e.g., Fig. 7(b), Fig. 7(c)) are applied on VH, which try to push it away from its current position. The time-varying torque field was generated by the equation given below:

$$\tau_{ext} = 5\sin\left(\frac{2\pi t}{60} + \frac{5\pi}{4} + \phi\right) + 5\sin\left(\frac{4\pi t}{60} + \frac{19\pi}{12} + \phi\right) + 10.3278, \tag{10}$$

where ϕ was set randomly from $[0, 2\pi)$ for each trial. The parameters were chosen such that the forces were out of phase with the desired trajectory, so as to make it difficult for the subjects to anticipate the magnitude of the disturbance. In addition, these parameters were chosen to be challenging but not overly frustrating for subjects. The subject was

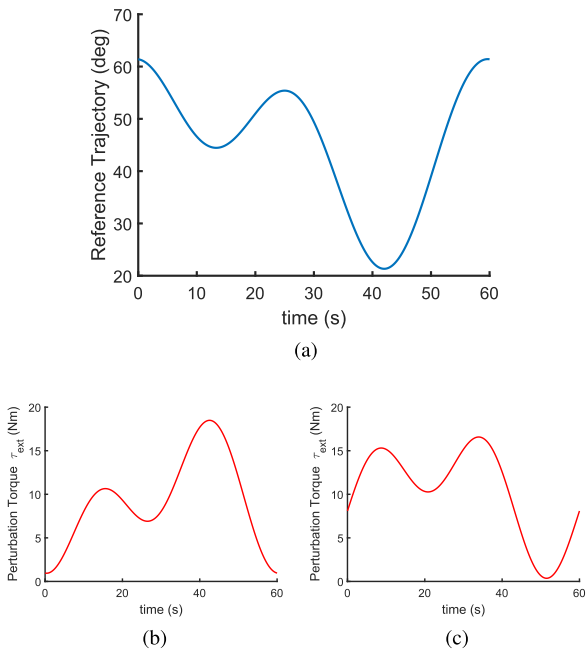

Fig. 7. The reference trajectory (a), the time-varying external perturbation torque with $\phi = 0$ (b) and $\phi = \pi/2$ (c) for the tracking task.

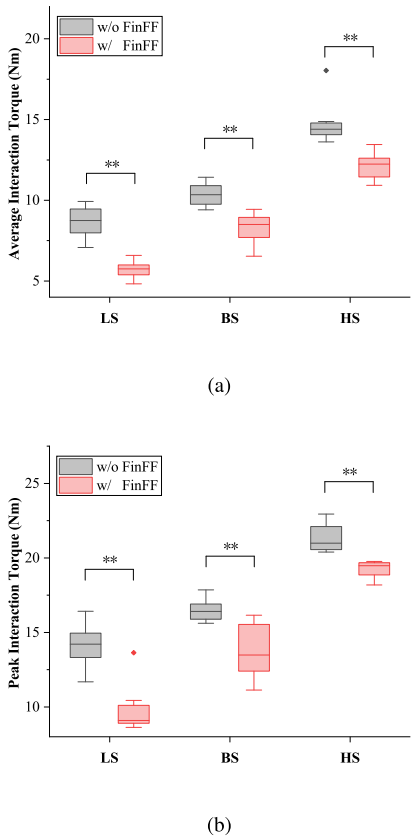

Fig. 8. Average interaction torques (a) and peak interaction torques (b) for the grasping task with and without wearable force feedback. The performance difference with statistical significance $p < 0.01$ is marked by "**."

instructed to make VH follow the goal trajectory while resist to randomly applied perturbation. We did not provide subjects any visual cues for the torque magnitude during the task, but the subject could perceive the perturbations via the haptic device as well as the deviation from the reference trajectory though vision. For calculating θ by Eq. (2) in this task, the equilibrium position θ_0 was set to 0. Two trials were recorded for each condition and each trial lasted 60 seconds. For the position tracking task, the root-mean-square error (RMSE) was adopted as the performance index.

V. Results

A. Grasping Task

Firstly, to determine the impact of wearable force feedback on the grasping torques under LS, HS and BS, the average interaction torques and the peak ones with and without FinFF are shown in Fig. 8. It shows the same general performance trend for the LS, HS and BS conditions: both the average and peak interaction torques are lower with FinFF than without. The Wilconxon signed rank test is then performed. It all shows statistically significant differences ($p < 0.01$) in average/peak interaction torques between the with FinFF and without FinFF conditions, for LS, HS and BS.

Next, since the interaction torques with FinFF are reduced w.r.t those without FinFF with statistical significance, results under LS, HS and BS with FinFF are further depicted in Fig. 9, so as to evaluate the effect of integrated usage of biomimetic impedance control and wearable finger haptic device on the performance. A Friedman test reveals statistically significant difference in the average interaction torques ($p < 0.001$) and the peak interaction torques ($p < 0.001$) between the three stiffness conditions. Post hoc analysis with pairwise Wilconxon signed-rank test (Hochberg correction for multiple comparisons) shows a statistically significant difference between BS vs. LS (average: $p = 0.0143$, peak: $p = 0.0143$), LS vs. HS (average: $p = 0.0143$, peak: $p = 0.0143$), BS vs. HS (average: $p = 0.0143$, peak: $p = 0.0143$). For the three stiffness conditions, LS exhibits the lowest interaction torques (average: 5.71 ± 0.53 Nm, peak: 9.81 ± 1.65 Nm), followed by BS (average: 8.28 ± 0.98 Nm, peak: 13.77 ± 1.82 Nm), and then HS (average: 12.12 ± 0.84 Nm, peak: 19.25 ± 0.59 Nm). It is worthwhile noting that the BS with FinFF scores relatively close to the LS with FinFF condition (difference in mean average torque: |BS-LS| = 2.57 Nm, |BS-HS| = 3.84 Nm), meaning that the BS condition tends to produce similar compliant grasps as the LS condition. Nevertheless, there were 3 failure trials out of the $4 \times 8 = 32$ attempts for 8 subjects under LS with FinFF, whereas no failure occurred under BS and HS with FinFF. With FinFF turned on, typical results of a failure trial under LS, representative results for a BS trial and a HS trial, are shown in Fig. 10. The estimated MCP joint angles and the interaction torques between VH and the object are shown. In addition, the subject's extensor and flexor muscular activities and stiffness index k_s under BS are given in the bottom-most plot. As can be seen from Fig. 10, on one hand, the LS controller produces interaction torques that are too low to successfully grasp the object. On the other hand, the HS condition leads to high grasp torques, which

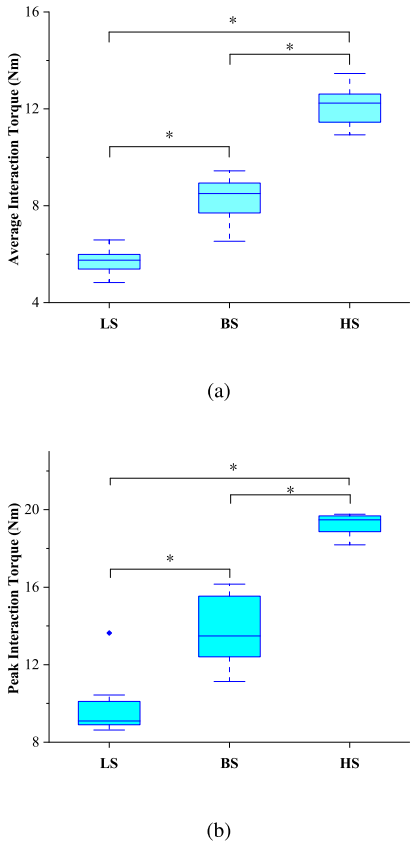

Fig. 9. Average interaction torques (a) and peak interaction torques (b) for the grasping task under different stiffness conditions with force feedback. The performance difference with statistical significance $0.01 < p < 0.05$ is marked by "*."

may prevent the subject from manipulating breakable or sharp virtual objects (e.g., eggs, needles) in serious games to be developed in future. In contrast to the LS and HS, user-driven modification of the VH stiffness in BS together with the FinFF, has provided compliant VH finger behaviors and successful grasps.

B. Position Tracking Task

Firstly, to investigate the strength of FinFF device for this task, we have performed the Wilconxon signed rank test on average RMSE under the two factors (with and without FinFF). As shown in Fig. 11, there is no statistically significant difference between the two factors under any stiffness condition ($p > 0.05$ for LS, BS and HS).

Secondly, to study the effect of stiffness condition on this task, we report the RMSE of FinFF-on trials under LS, BS and HS in Fig. 12. The smallest tracking error is achieved with HS (2.00 ± 0.67 deg), BS scores the second (2.5 ± 0.56 deg) and LS has the largest error (3.25 ± 0.49 deg). With the Friedman test, we finds that there is a statistically significant difference in RMSE between the stiffness conditions ($p = 0.003$). Post hoc analysis with Wilconxon signed rank test (Hochberg correction for multiple comparisons) shows that both HS and BS significantly improve the tracking accuracy over the LS condition (HS vs. LS: $p = 0.0209$, BS vs. LS: $p = 0.0209$).

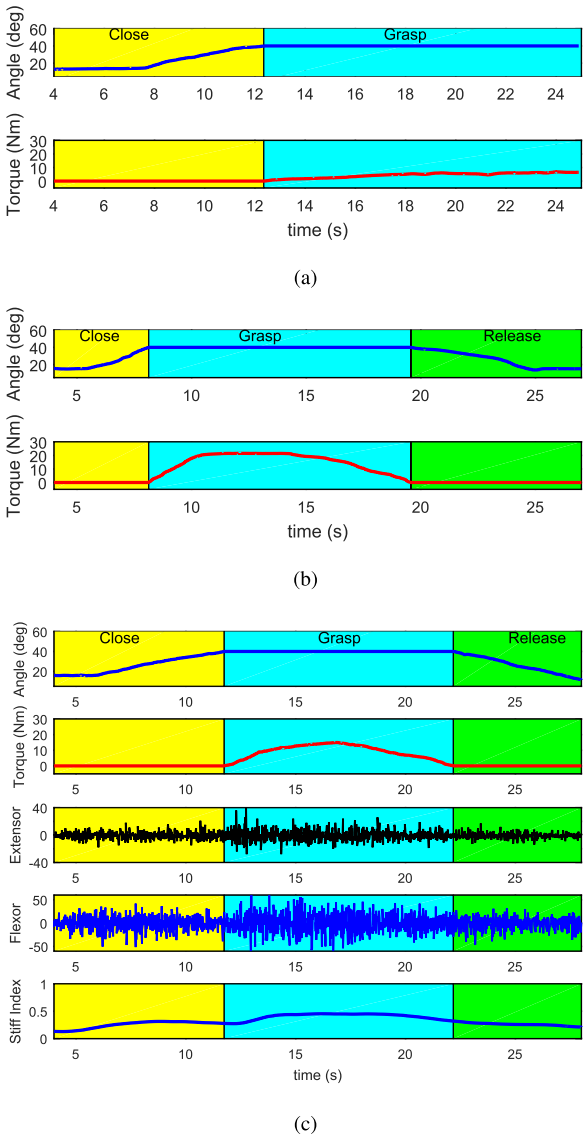

Fig. 10. A typical trial of a representative subject for the grasping task under different stiffness conditions with force feedback. (a) low, fixed stiffness (b) high, fixed stiffness (c) biomimetically modulated stiffness.

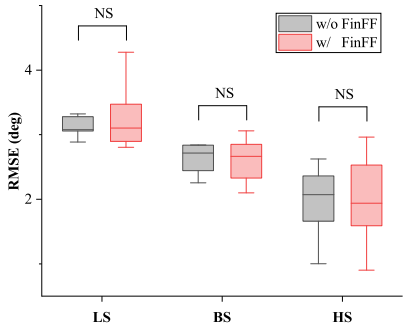

Fig. 11. RMSE for the tracking task with and without wearable force feedback. The non-significant difference is marked by "NS."

Besides, there is no statistical difference between BS and the HS condition ($p = 0.0587$). A typical trial of one subject performing the tracking task under LS, BS and HS, is shown

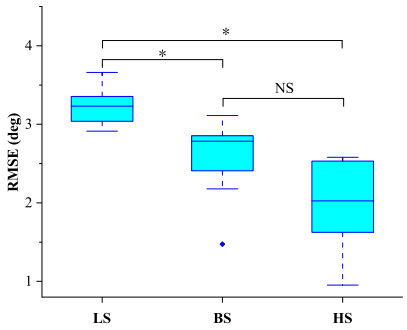

Fig. 12. RMSE for the tracking task under different stiffness conditions with force feedback.

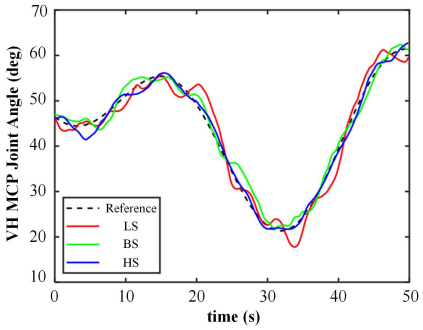

Fig. 13. A typical trial of a representative subject for the tracking task, under fixed low stiffness, fixed high stiffness, and biomimetically modulated stiffness with force feedback.

in Fig. 13. As shown in Fig.13, the HS condition generally produces precise path-following movements, whereas the VH under the LS condition is too soft that it results in large deviations, especially after the peak and valley of the reference trajectory. Besides, the behavior of VH under BS condition resembles that under HS.

C. Performance Aggregation for the Two Tasks

Toward showing a comprehensive and cohesive picture of the VH behaviors with our presented integrated solution, the aggregated performance metrics for the grasping (average interaction torque) and position tracking (RMSE) tasks are shown in Fig. 14. As demonstrated in Fig. 14, the performance metrics majorities (expanding from the 25th percentile to the 75th percentile) by BS with FinFF score relatively close to those by the optimal condition for the grasping task, i.e., LS with FinFF, while they are relatively close to those by the optimal HS condition for the position tracking task.

VI. Discussions

A. Task-Desired VH Behaviors Attained by Our Solution

Regarding the grasping task, results have confirmed that force feedback can enhance VH grasp force control based on impedance model when vision is occuled. It is necessary to point out that we did not provide any visual cue regarding the amount of force to apply when grasping an object. Offering the kinesthetic feedback instead of the tactile one, the FinFF device is able to elicit a natural and compelling

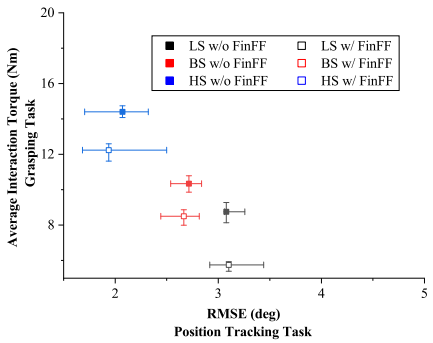

Fig. 14. Task performance with different stiffness levels and FinFF-on/off options. The square marker denote the median value. The whiskers extend to the 25th and 75th percentile.

feeling of contact in VR. Accordingly, such information makes the subject decrease the muscular activities around the joint, and then the impedance control scheme naturally leads to smaller interaction torques between VH and the object compared to the trials without FinFF. The stiffness conditions have also demonstrated significant effects on grasping performance. On one hand, we have observed that trials under the condition with fixed low stiffness and FinFF are subject to failures in ensuring an adequate grip. This may be ascribed to two reasons. Firstly, the torque produced with the impedance model in LS condition is lower compared to the other two. Secondly, the force cues conveyed by the FinFF may further drive the user to reduce the muscle contraction. On the other hand, considering the HS condition with FinFF, the impedance control model has resulted in strong VH finger movements. These movements have generated high grasping torques that can be regulated with difficulty, even with the employment of FinFF. By contrast, the integrated usage of biomimetic impedance control and wearable finger force-feedback device has produced a different modulation of the interaction torques, which are generally lower w.r.t HS and higher w.r.t LS. This would result in more compliant and energy-efficient grasps compared to the HS case, while would be more likely to increase the chances of success trial rate in comparison to the LS case.

Note in the position tracking experiment, the subject could perceive not only the perturbation torque via FinFF, but also the visual feedback about the displacement between VH (the white dot in Fig. 5 (c)) and the desired trajectory. To mitigate the dominance of the visual feedback in the integrated visual-haptic perception, the projection of VH, i.e., the white dot in Fig. 5 (c), was designed to be quite small on purpose, so that subjects would not ignore the perturbation torque provided by FinFF but relying solely on vision. As expected, the HS condition leads to significantly better performance than the LS condition, since a high stiffness level in the impedance controller is known to be effective for compensating the time-varying disturbance and completing an accurate tracking. Under the BS condition, the subject is adaptively driven to increase his/her stiffness with the integrated perception from the VR environment, and then the biomimetic impedance control scheme naturally produces precise VH's joint movements similar to the HS condition without statistically significant difference.

However, the current study showed an insignificant reduction of tracking RMSE with force feedback compared to without force feedback, possibly due to the limited practice with FinFF for subjects. As previous studies [3], [17] have pointed out that haptic device training for users is important for skill learning, future work will expand the evaluations of the FinFF's impact on VH tracking behavior in a longer time-scale with blocks of trials. Not including force feedback to the subject, the "BS w/o FinFF" condition produces rigid behavior for accurate tracking, whereas it greatly lacks transparency. The FinFF could increase subjects' situational awareness, providing them an immersive sensation of the perturbation torques on VH in addition to the position signals.

Putting the results in two tasks together, the following remarks are made. Although the aggregated performance metrics in Fig. 14 show that the biomimetic impedance control without haptic feedback has provided a solution to derive task-adaptive interaction behaviors, which are in line with the literature [24], [25], the integration of wearable force feedback with biomimetic impedance control further shifts the performance metrics under BS condition toward the bottom left corner of the coordinate system in Fig. 14. Namely, adding a natural haptic sensory feedback channel in myoelectric control of VH is helpful for the subject to gain enhanced perception of VR environment with vision alone, which facilitates the subject to voluntarily adjust the stiffness gains in impedance control paradigm for VH. In other words, our solution improves over the partial solution by biomimetic impedance control alone, representing an important step forward in promoting VH to adaptively produce task-appropriate interaction behaviors like human hands.

B. Limitations and Future Work

The work presented in this paper may facilitate the future development of immersive embodied serious games for rehabilitative training hand's motor skills, e.g., games that require specific stiffness profiles. Learning delicate stiffness modulation is very important in successfully performing certain activities of daily living. A further consideration for application to VR rehabilitation training is control over multiple degrees of freedom. In this work, we have only considered the simplest one-DoF system, aiming at verifying the benefits of biomimetic impedance control with wearable haptics for representative tasks. We plan to address the multiple-DoF control issue in future work. Another consideration for application to VR rehabilitation training is the online determination of EMG-related parameters to avoid prior tests. The current system is not a plug-and-play one, as biomimetic impedance control requires an initial user-dependent calibration, which will also be addressed in future.

VII. Conclusion

In this paper, we have presented a myoelectric-controlled VH system which subsumes the advantages of biomimetic stiffness modulation and wearable finger haptics. The proposed approach has been verified in two tasks with opposite behavior requirements for impedance control of VH. Results reveal that the integrated interface has provided compliant VH behaviors and increased success chance for the grasping task, while it also has obtained stiff VH behaviors for the position tracking task. Namely, without user consciously selecting the VH mode of operation for different tasks, VH attains human-like task-dependent behaviors via the fusion of effective biomimetic impedance control and intuitive fingertip force feedback. This proof-of-concept work has the potential for improving the embodiment of VH by the user, which is important for VR-based hand rehabilitation applications.

References

[1] M. Ison, I. Vujaklija, B. Whitsell, D. Farina, and P. Artemiadis, "High-density electromyography and motor skill learning for robust long-term control of a 7-DoF robot arm," *IEEE Trans. Neural Syst. Rehabil. Eng.*, vol. 24, no. 4, pp. 424–433, Apr. 2015.

[2] D. T. Kluger *et al.*, "Virtual reality provides an effective platform for functional evaluations of closed-loop neuromyoelectric control," *IEEE Trans. Neural Syst. Rehabil. Eng.*, vol. 27, no. 5, pp. 876–886, May 2019.

[3] E. Basalp, P. Wolf, and L. Marchal-Crespo, "Haptic training: Which types facilitate (re) learning of which motor task and for whom? Answers by a review," *IEEE Trans. Haptics*, vol. 14, no. 4, pp. 722–739, Oct. 2021.

[4] M. F. Montoya, J. E. Munoz, and O. A. Henao, "Enhancing virtual rehabilitation in upper limbs with biocybernetic adaptation: The effects of virtual reality on perceived muscle fatigue, game performance and user experience," *IEEE Trans. Neural Syst. Rehabil. Eng.*, vol. 28, no. 3, pp. 740–747, Mar. 2020.

[5] I. Bortone *et al.*, "Wearable haptics and immersive virtual reality rehabilitation training in children with neuromotor impairments," *IEEE Trans. Neural Syst. Rehabil. Eng.*, vol. 26, no. 7, pp. 1469–1478, Jul. 2018.

[6] J. W. Choi, B. H. Kim, S. Huh, and S. Jo, "Observing actions through immersive virtual reality enhances motor imagery training," *IEEE Trans. Neural Syst. Rehabil. Eng.*, vol. 28, no. 7, pp. 1614–1622, Jul. 2020.

[7] S. Bovet, H. G. Debarba, B. Herbelin, E. Molla, and R. Boulic, "The critical role of self-contact for embodiment in virtual reality," *IEEE Trans. Vis. Comput. Graphics*, vol. 24, no. 4, pp. 1428–1436, Apr. 2018.

[8] D. Perez-Marcos, "Virtual reality experiences, embodiment, videogames and their dimensions in neurorehabilitation," *J. Neuroeng. Rehabil.*, vol. 15, no. 1, pp. 1–8, Dec. 2018.

[9] A. Boschmann, D. Neuhaus, S. Vogt, C. Kaltschmidt, M. Platzner, and S. Dosen, "Immersive augmented reality system for the training of pattern classification control with a myoelectric prosthesis," *J. Neuroeng. Rehabil.*, vol. 18, no. 1, pp. 1–15, Dec. 2021.

[10] X. Zhang, G. Zhu, M. Chen, X. Chen, X. Chen, and P. Zhou, "Muscle force estimation based on neural drive information from individual motor units," *IEEE Trans. Neural Syst. Rehabil. Eng.*, vol. 28, no. 12, pp. 3148–3157, Dec. 2020.

[11] A. Tabor, S. Bateman, and E. Scheme, "Evaluation of myoelectric control learning using multi-session game-based training," *IEEE Trans. Neural Syst. Rehabil. Eng.*, vol. 26, no. 9, pp. 1680–1689, Sep. 2018.

[12] Z. Lu, K.-Y. Tong, X. Zhang, S. Li, and P. Zhou, "Myoelectric pattern recognition for controlling a robotic hand: A feasibility study in stroke," *IEEE Trans. Biomed. Eng.*, vol. 66, no. 2, pp. 365–372, Feb. 2019.

[13] M. Ghassemi *et al.*, "Development of an EMG-controlled serious game for rehabilitation," *IEEE Trans. Neural Syst. Rehabil. Eng.*, vol. 27, no. 2, pp. 283–292, Feb. 2019.

[14] A. Dash and U. Lahiri, "Design of virtual reality-enabled surface electromyogram-triggered grip exercise platform," *IEEE Trans. Neural Syst. Rehabil. Eng.*, vol. 28, no. 2, pp. 444–452, Feb. 2019.

[15] M. Rietzler, G. Haas, T. Dreja, F. Geiselhart, and E. Rukzio, "Virtual muscle force: Communicating kinesthetic forces through pseudo-haptic feedback and muscle input," in *Proc. 32nd Annu. ACM Symp. User Interface Softw. Technol.*, Oct. 2019, pp. 913–922.

[16] G. Nakamura *et al.*, "A virtual myoelectric prosthesis training system capable of providing instructions on hand operations," *Int. J. Adv. Robotic Syst.*, vol. 14, no. 5, Sep. 2017, Art. no. 1729881417728452.

[17] A. A. Blank, A. M. Okamura, and L. L. Whitcomb, "Task-dependent impedance and implications for upper-limb prosthesis control," *Int. J. Robot. Res.*, vol. 33, no. 6, pp. 827–846, May 2014.
[18] E. Burdet, R. Osu, D. W. Franklin, T. E. Milner, and M. Kawato, "The central nervous system stabilizes unstable dynamics by learning optimal impedance," *Nature*, vol. 414, pp. 446–449, Nov. 2001.
[19] R. D. Trumbower and C. Tuthill, "Neural regulation of whole limb impedance: From measurements to mechanisms," *Current Opinion Physiol.*, vol. 22, Aug. 2021, Art. no. 100437.
[20] P. E. Dupont *et al.*, "A decade retrospective of medical robotics research from 2010 to 2020," *Sci. Robot.*, vol. 6, no. 60, Nov. 2021, Art. no. eabi8017.
[21] V. R. Garate, S. Gholami, and A. Ajoudani, "A scalable framework for multi-robot tele-impedance control," *IEEE Trans. Robot.*, vol. 37, no. 6, pp. 2052–2066, Dec. 2021.
[22] M. Laghi, A. Ajoudani, M. G. Catalano, and A. Bicchi, "Unifying bilateral teleoperation and tele-impedance for enhanced user experience," *Int. J. Robot. Res.*, vol. 39, no. 4, pp. 514–539, Mar. 2020.
[23] A. Ajoudani *et al.*, "Exploring teleimpedance and tactile feedback for intuitive control of the pisa/iit softhand," *IEEE Trans. Haptics*, vol. 7, no. 2, pp. 203–215, Mar. 2014.
[24] A. Ajoudani, N. Tsagarakis, and A. Bicchi, "Tele-impedance: Teleoperation with impedance regulation using a body–machine interface," *Int. J. Robot. Res.*, vol. 31, no. 13, pp. 1642–1656, 2012.
[25] W. Gallagher, D. Gao, and J. Ueda, "Improved stability of haptic human–robot interfaces using measurement of human arm stiffness," *Adv. Robot.*, vol. 28, no. 13, pp. 869–882, Jul. 2014.
[26] M. Laghi, A. Ajoudani, M. Catalano, and A. Bicchi, "Tele-impedance with force feedback under communication time delay," in *Proc. IEEE/RSJ Int. Conf. Intell. Robots Syst. (IROS)*, Sep. 2017, pp. 2564–2571.
[27] S. Fani *et al.*, "Simplifying telerobotics: Wearability and teleimpedance improves human-robot interactions in teleoperation," *IEEE Robot. Autom. Mag.*, vol. 25, no. 1, pp. 77–88, Mar. 2018.
[28] J. P. Clark, G. Lentini, F. Barontini, M. G. Catalano, M. Bianchi, and M. K. O. Malley, "On the role of wearable haptics for force feedback in teleimpedance control for dual-arm robotic teleoperation," in *Proc. Int. Conf. Robot. Autom. (ICRA)*, May 2019, pp. 5187–5193.
[29] C. Pacchierotti, S. Sinclair, M. Solazzi, A. Frisoli, V. Hayward, and D. Prattichizzo, "Wearable haptic systems for the fingertip and the hand: Taxonomy, review, and perspectives," *IEEE Trans. Haptics*, vol. 10, no. 4, pp. 580–600, Oct./Dec. 2017.
[30] D. Prattichizzo, M. Otaduy, H. Kajimoto, and C. Pacchierotti, "Wearable and hand-held haptics," *IEEE Trans. Haptics*, vol. 12, no. 3, pp. 227–231, Jul. 2019.
[31] D. Leonardis, M. Solazzi, I. Bortone, and A. Frisoli, "A 3-RSR haptic wearable device for rendering fingertip contact forces," *IEEE Trans. Haptics*, vol. 10, no. 3, pp. 305–316, Jul./Sep. 2016.
[32] F. H. Giraud, S. Joshi, and J. Paik, "Haptigami: A fingertip haptic interface with vibrotactile and 3-DoF cutaneous force feedback," *IEEE Trans. Haptics*, vol. 15, no. 1, pp. 131–141, Jan. 2021.
[33] F. Chinello, M. Malvezzi, D. Prattichizzo, and C. Pacchierotti, "A modular wearable finger interface for cutaneous and kinesthetic interaction: Control and evaluation," *IEEE Trans. Ind. Electron.*, vol. 67, no. 1, pp. 706–716, Jan. 2019.
[34] H. A. Sonar, J.-L. Huang, and J. Paik, "Soft touch using soft pneumatic actuator–skin as a wearable haptic feedback device," *Adv. Intell. Syst.*, vol. 3, no. 3, Mar. 2021, Art. no. 2000168.
[35] A. Z. Hajian and R. D. Howe, "Identification of the mechanical impedance at the human finger tip," *J. Biomech. Eng.*, vol. 119, no. 1, pp. 109–114, Feb. 1997.
[36] S. Hilt, T. Meunier, C. Pontonnier, and G. Dumont, "Biomechanical fidelity of simulated pick- and-place tasks: Impact of visual and haptic renderings," *IEEE Trans. Haptics*, vol. 14, no. 3, pp. 692–698, Jul. 2021.
[37] A. Pallotti, G. Orengo, and G. Saggio, "Measurements comparison of finger joint angles in hand postures between an sEMG armband and a sensory glove," *Biocybernetics Biomed. Eng.*, vol. 41, no. 2, pp. 605–616, Apr. 2021.
[38] A. Furui *et al.*, "A myoelectric prosthetic hand with muscle synergy–based motion determination and impedance model–based biomimetic control," *Sci. Robot.*, vol. 4, no. 31, Jun. 2019, Art. no. eaaw6339.
[39] H. S. Milner-Brown and R. B. Stein, "The relation between the surface electromyogram and muscular force," *J. Physiol.*, vol. 246, no. 3, pp. 549–569, Apr. 1975.
[40] Y. Mo, A. Song, H. Qin, and Y. Yu, "Method and system of wearable fingertip force/tactile feedback with dual-channel," *Chin. J. Sci. Instrum.*, vol. 39, no. 11, pp. 188–194, 2018.